Coupled Stratospheric Ozone and Atlantic Meridional Overturning Circulation Feedbacks on the Northern Hemisphere Midlatitude Jet Response to 4xCO_2

Clara Orbe[a,b] , David Rind[a] , Darryn Waugh[c] , Jeffrey Jonas[a,d] , Xiyue Zhang[c] , Gabriel Chiodo[e] , Larissa Nazarenko[a,d] , and Gavin A. Schmidt[a]

[a] *NASA Goddard Institute for Space Studies, New York, NY*

[b] *Department of Applied Physics and Applied Mathematics, Columbia University, New York, NY*

[c] *Department of Earth and Planetary Sciences, Johns Hopkins University, Baltimore, MD*

[d] *Center for Climate Systems Research, Earth Institute, Columbia University, New York, NY*

[e] *Institute for Atmospheric and Climate Science, ETH Zurich, Switzerland*

Corresponding author: Clara Orbe, clara.orbe@nasa.gov

ABSTRACT: Stratospheric ozone, and its response to anthropogenic forcings, provide an important pathway for the coupling between atmospheric composition and climate. In addition to stratospheric ozone's radiative impacts, recent studies have shown that changes in the ozone layer due to $4xCO_2$ have a considerable impact on the Northern Hemisphere (NH) tropospheric circulation, inducing an equatorward shift of the North Atlantic jet during boreal winter. Here we show that this equatorward jet shift can induce a more rapid weakening of the Atlantic Meridional Overturning Circulation (AMOC), resulting in a poleward shift of the midlatitude eddy-driven jet on longer timescales. As such, coupled feedbacks from both stratospheric ozone and the AMOC result in a two-timescale response of the NH midlatitude jet to abrupt $4xCO_2$ forcing: a "fast" response (5-20 years) during which it shifts equatorward and a "total" response (~100-150 years) during which the jet shifts poleward. The latter is driven by a weakening of the AMOC that develops in response to weaker surface zonal winds, that result in reduced heat fluxes out of the subpolar gyre and reduced North Atlantic Deep Water formation. Our results suggest that stratospheric ozone changes in the lower stratosphere can have a surprisingly powerful effect on the AMOC, independent of other aspects of climate change.

1. Introduction

There is large uncertainty in the atmospheric circulation response to increasing greenhouse gases (see Shepherd (2014) and references therein). Although models generally predict a poleward shift of the midlatitude eddy-driven jet, the magnitude of this shift is highly uncertain (e.g., Vallis et al. (2015); Grise and Polvani (2014)) as are its underlying drivers (Shaw (2019)). This is especially true in the Northern Hemisphere (NH), where there are opposing thermodynamic influences, i.e. opposite meridional temperature gradient responses at the surface versus the upper troposphere (Shaw et al. (2016)). Thus, while enhanced warming in the lower polar troposphere relative to the lower tropical troposphere (i.e., Arctic amplification) contributes to reduced meridional temperature gradients, increases in upper tropospheric tropical warming contribute to enhanced temperature gradients aloft (Butler et al. (2010); Yuval and Kaspi (2020)) and it is not clear how these competing processes affect the zonal mean midlatitude jet.

Many processes have been shown to influence the response of meridional temperature gradients to increased CO_2, including polar amplification (see Smith et al. (2019) and references therein) and cloud feedbacks (e.g., Ceppi and Hartmann (2015); Voigt and Shaw (2015)). By comparison, composition feedbacks associated with the ozone response to CO_2 have been less well examined although stratospheric ozone changes have been identified as an important pathway coupling composition to climate (Isaksen et al. (2009)). In particular, the stratospheric ozone response to $4xCO_2$ consists of robust decreases in the tropical lower stratosphere (LS), increases in the tropical upper stratosphere and increases over high latitudes (Chiodo et al. (2018)). While the exact details of these changes are model dependent, especially over high latitudes, the general pattern is very consistent among models (e.g., Nowack et al. (2015); Chiodo et al. (2018) and Chiodo and Polvani (2019) (hereafter CP2019)).

This pattern of reduced (increased) ozone over the tropical (high latitude) LS in response to $4xCO_2$ has immediate implications for temperature gradients in the stratosphere by cooling the tropics and warming high latitudes (Nowack et al. (2015); Chiodo et al. (2018); Li and Newman (2022)). As CP2019 and Li and Newman (2022) showed, these changes in temperature gradients drive an anomalous equatorward shift of the midlatitude jet in the Southern Hemisphere (SH). In addition, both studies also showed shifts in the Northern Hemisphere (NH), where anomalies

extend down into the lower troposphere and are concentrated over the Atlantic, resembling the negative phase of the North Atlantic Oscillation (NAO).

A more recent study by Zhang et al. (2023), that considered two models that differed only in their representation of interactive chemistry, also showed that changes in composition can impact the sign of the NH midlatitude jet response to increased CO_2. However, in contrast to CP2019, the long-term impact of this composition feedback was a *poleward*, not equatorward, shift of the NH jet. Though not investigated in detail, this poleward shift of the jet was linked to changes in the ocean circulation, which were not examined in CP2019. More precisely, Zhang et al. (2023) noted that the Atlantic Meridional Overturning Circulation (AMOC) exhibited a stronger decline in interactive simulations in which trace gases and aerosols were allowed to respond to increased CO_2, relative to non-interactive simulations. Indeed, recent studies have highlighted the large influence that changes in the AMOC exert on the response of the NH midlatitude jet to increased CO_2 (Gervais et al. (2019)), with models featuring a larger AMOC decline also tending to produce a stronger poleward jet shift (Bellomo et al. (2021); Liu et al. (2020); Orbe et al. (2023)).

The results from Zhang et al. (2023) suggest that composition feedbacks on the NH midlatitude jet may depend on the response of the ocean circulation. However, that study did not examine the mechanism underlying the stronger AMOC response in the interactive chemistry simulations nor did it isolate the role of ozone from influences due to other trace gases and aerosols. To this end, here we hypothesize that the ozone-induced negative NAO wind anomalies reported in CP2019 provide a potential pathway through which stratospheric ozone changes can influence the AMOC and the long-term response of the NH midlatitude jet. Our hypothesis is partly predicated on results from previous studies showing that variations in the jet – namely those resembling the NAO – can influence variability of the AMOC through changes in wind stress (Marshall et al. (2001); Zhai and Marshall (2014)). Modified air-sea fluxes of heat, water and momentum associated with variations in the NAO alter vertical and horizontal density gradients in the subpolar gyre, inducing changes in deep water formation and the AMOC (e.g., Visbeck et al. (1998); Delworth and Dixon (2000)). This pathway via the NAO has been used to demonstrate how sudden stratospheric warmings influence the variability of heat flux anomalies into the ocean and ocean mixed layer depths in the North Atlantic (O'Callaghan and Mitchell (2014)) as well as the strength of the AMOC itself (Reichler et al. (2012)).

Here we present results from non-interactive and fully interactive chemistry global warming experiments produced with the new high-top coupled atmosphere ocean version of the NASA Goddard Institute for Space Studies (GISS) climate model that were submitted to the Coupled Model Intercomparison Project Phase 6 (CMIP6) (Eyring et al. (2016)). We focus on simulations in which CO_2 is abruptly doubled and quadrupled in order to facilitate comparison with the results presented in CP2019 and Zhang et al. (2023).

We begin by verifying that reduced ozone in the tropical lower stratosphere, which is captured only in the interactive simulations, leads to an equatorward shift of the midlatitude jet on relatively fast timescales. Then we show that the AMOC response in the interactive simulations is largely associated with these ozone-driven changes in the jet, not aerosols, using new experiments in which the stratospheric ozone response to $4xCO_2$ is isolated from changes in other trace gases and aerosols. In particular, we show that our model captures the ozone-induced negative NAO-like pattern first reported in CP2019; in addition, we also find that ozone-driven changes in surface friction speed further weaken the AMOC, resulting in a long-term poleward shift of the NH jet. As a result, we show that both stratospheric ozone changes and the AMOC influence the NH jet on distinct "fast" and "total" timescales (and in the opposite sense), comprising a coupled atmosphere-ocean feedback on the NH midlatitude jet response to increased CO_2. While the former "fast" feedback was documented in CP2019, the latter has, to the best of our knowledge, not been reported in previous studies.

It is important to note that previous studies have long shown that interactive atmospheric composition can strongly influence the AMOC, placing an almost exclusive focus on the role of aerosols (Booth et al. (2012); Cowan and Cai (2013); Swingedouw et al. (2015)). More recently, Rind et al. (2018) also identified a larger sensitivity of the AMOC response to global warming using an interactive configuration of the CMIP5 version of the GISS climate model (GISS-E2-R), compared to a non-interactive version. In that study, multicentennial cessations of the AMOC were found to occur in simulations in which natural aerosols (primarily sea salt) were allowed to locally cool sea surface temperatures through their influence on cloud optical thickness; these cooler SSTs were then linked to reduced evaporation relative to precipitation, resulting in positive surface freshwater forcing and reduced NADW production. As in Rind et al. (2018) we also show that composition feedbacks play an important role on the response of the AMOC to CO_2 through their influence

on surface fluxes and surface temperatures. However, the mechanism proposed here only invokes changes in stratospheric ozone, not aerosols. We begin by discussing methods in Section 2 and then present key results and conclusions in Sections 3 and 4, respectively.

2. Methods

a. Model and Configurations

Here we use the NASA Goddard Institute for Space Studies (GISS) "Middle Atmosphere (MA)" Model E2.2 (Rind et al. (2020); Orbe et al. (2020)). E2.2 consists of 102 vertical levels spanning the surface up to 0.002 hPa and is run at a horizontal resolution of 2 degrees by 2.5 degrees. Orographic and non-orographic gravity wave drag is parameterized following Lindzen (1987) and Rind et al. (1988), producing in E2.2 a quasibiennial oscillation (QBO) that compares well with observations as well as improved stratospheric polar vortex variability (Ayarzagüena et al. (2020); Rind et al. (2020)). Of most relevance to this study, Orbe et al. (2020) showed that E2.2 produces a significantly improved representation of the Brewer-Dobson and stratospheric transport circulations, compared to the lower vertical resolution CMIP6 version of ModelE (E2.1, Kelley et al. (2020)), resulting in reduced biases in ozone, methane, water vapor and nitrous oxide (see their Figure 1). Among the different model versions discussed in Rind et al. (2020) and Orbe et al. (2020) here we focus on the "Altered-Physics" (-AP) Version (E2.2-AP) because this is the configuration that was submitted to CMIP6 and presented in recent studies (Ayarzagüena et al. (2020); DallaSanta et al. (2021a,b)).

We begin by showing the results reported in Zhang et al. (2023) using both "Non-INTeractive" (NINT) (Table 1, rows 1-3) and fully interactive "One-Moment Aerosols" (OMA) (Bauer et al. (2020); Table 1, rows 4-6) configurations. In the NINT configuration all trace gases and aerosols are set to preindustrial values. Hence, in the 2- and 4xCO_2 NINT runs neither ozone nor other trace gases (besides water vapor) change in response to increased CO_2. By comparison, the OMA 2- and 4xCO_2 runs capture the full nonlinear ozone response to CO_2, as well as composition feedbacks associated with other trace gases and aerosols.

In order to isolate the role of ozone feedbacks on the circulation, we then perform experiments using a linearized ozone (LINOZ) configuration (Table 1, rows 7-9). In LINOZ the ozone field is calculated interactively by Taylor expanding the equation of state around present-day (2000–2010)

TABLE 1. The Model E2.2 experiments presented in this study, including preindustrial control, abrupt 2xCO_2 and abrupt 4xCO_2 simulations using NINT (rows 1-3), OMA (rows 4-6) and LINOZ (rows 7-9) configurations. Four NINT abrupt 4xCO_2 ensemble members are included (row 3) in order to compare with a four member 4xCO_2 ensemble produced using the LINOZ configuration (row 8). The 4xCO_2 ensemble mean LINOZ ozone response is also used to force four prescribed SST and SIC preindustrial experiments (row 10) in which all forcings other than ozone are set to preindustrial values. All coupled atmosphere-ocean simulations are run using the GISS Ocean v1 (GO1) (i.e., "-G" in CMIP6 notation).

Configuration	Ozone	CO_2	Ensemble Size	SSTs and SICs
NINT	Preindustrial	Preindustrial	1	coupled (-G ocean)
NINT	Preindustrial	2xCO_2	1	coupled (-G ocean)
NINT	Preindustrial	4xCO_2	4	coupled (-G ocean)
OMA	Preindustrial	Preindustrial	1	coupled (-G ocean)
OMA	2xCO_2	2xCO_2	1	coupled (-G ocean)
OMA	4xCO_2	4xCO_2	1	coupled (-G ocean)
LINOZ	Preindustrial	Preindustrial	1	coupled (-G ocean)
LINOZ	2xCO_2	2xCO_2	1	coupled (-G ocean)
LINOZ	4xCO_2	4xCO_2	4	coupled (-G ocean)
NINT	LINOZ 4xCO_2	Preindustrial	4	Prescribed Preindustrial

values such that the ozone tendency is, to first-order, parameterized as a function of the local ozone mixing ratio, temperature, and overhead column ozone (McLinden et al. (2000)). Tropospheric ozone is calculated using monthly mean ozone production and loss rates archived from GEOS-CHEM (Rind et al. (2014)). In contrast to NINT, therefore, the LINOZ ensemble captures the influence of the ozone response to CO_2 on the large-scale circulation. Unlike OMA, however, it is much more computationally efficient to run and isolates the ozone feedback from feedbacks related to other trace gases and aerosols. DallaSanta et al. (2021a) previously showed that the LINOZ ozone parameterization reproduces well the vertical structure and seasonal cycle of stratospheric ozone obtained from the fully interactive OMA configuration (see their Figure 1).

b. Experiments

For the different model configurations (NINT, OMA, LINOZ) we perform 150-year-long abrupt 2- and 4xCO_2 experiments, in which CO_2 values are abruptly doubled and quadrupled relative to preindustrial concentrations. For each model configuration, these experiments are branched from

a corresponding preindustrial control simulation. For NINT and LINOZ four-member 4xCO_2 ensembles are run in order to assess the robustness of any ozone feedbacks. These experiments are all conducted using the atmosphere-ocean version of E2.2-AP that is coupled to the GISS Ocean v1 (GO1) (i.e., "-G" in CMIP6 notation, hereafter simply E2.2-G). For coupled atmosphere-ocean configurations in which (four-member) ensembles are run, different ensemble members are chosen from different initial ocean states spaced 20 years apart in the corresponding preindustrial control simulation.

In addition to the coupled atmosphere-ocean experiments, we also present results from a four-member ensemble of 60-year-long atmosphere-only experiments in which sea surface temperatures (SSTs) and sea ice concentrations (SICs) are fixed to preindustrial values, but the monthly mean time-evolving ensemble mean ozone response from the coupled LINOZ 4xCO_2 experiments is prescribed (Table 1, row 10). This allows us to quantify the impact of the ozone feedback represented in LINOZ on the large-scale circulation, absent any contributions from changes in background CO_2, sea ice concentrations or sea surface temperatures.

c. Analysis

1) Timescales

When examining the midlatitude jet response to increased CO_2 we account for the fact that extratropical circulation changes consist of distinct "fast" and "slow" responses (Ceppi et al. (2018), hereafter CZS2018). More precisely, CZS2018 show that most of the shift of the midlatitude jets occurs within 5-10 years of a steplike (abrupt) CO_2 forcing, with little shifts occurring during a slower response over which SSTs change over subsequent decades. In contrast to the Southern Hemisphere, zonal asymmetries play an important role in the Northern Hemisphere, where the influence of local patterns in sea surface temperature change can result in oppositely signed jet shifts on "slow" timescales. Given this potential for compensating jet shifts on distinct timescales, we therefore decompose the CO_2 circulation response into "fast" and "total" timescale responses.

More precisely, to account for the large internal variability in our runs, perhaps related to a somewhat larger ENSO amplitude in our model compared to observations (Rind et al. (2020)), we modify the original approach used in CZS2018 to define our "fast" response as the difference between the ensemble mean 4xCO_2 response, averaged over years 5-20 (as opposed to years 5-10),

and the corresponding preindustrial control simulation. In addition, instead of focusing on the "slow" response, defined in CZS2018 as the difference between averages over years 121-140 and years 5-10, here we examine the "total" response, defined as the difference between the ensemble mean 4xCO_2 response, averaged over years 100-150, and the preindustrial control simulation. This approach is more consistent with what was used in Zhang et al. (2023) and CP2019, with which we directly compare our results throughout. Note that in response to an abrupt quadrupling of CO_2 the NINT model configuration produces global mean surface temperature "fast" and "total" responses of ~2.9°C and ~3.9°C, respectively. Statistical significance is assessed using a two-sample Student's t-test comparing all abrupt CO_2 changes to the interannual variability in the corresponding preindustrial control simulation for each configuration (Table 1, rows 1,4,7).

2) Analysis Fields

In addition to the atmospheric variables examined in CP2019 (i.e., zonal mean wind, zonal mean temperature, surface temperature, 850 hPa zonal wind) we examine ocean variables relevant to understanding the evolution of the AMOC and its coupling to the atmosphere. In particular, in addition to examining the surface mixed layer depths we also examine sea surface temperatures, surface friction speed, horizontal ocean heat and salinity transports, as well as the net heat fluxes which, together with the net freshwater fluxes (F; inferred from precipitation minus evaporation (P-E)), provide information about the surface buoyancy forcing (Large and Yeager (2009)). In our simulations, the preindustrial climatological buoyancy forcing over the North Atlantic is dominated by the sum of the net heat fluxes ($Q = Q_H+Q_E+Q_S+Q_L$), which are defined to be positive into the ocean (Appendix Figure A1, left). These are further partitioned into their respective latent heat (Q_E) and sensible heat (Q_H) contributions as we find that the net solar (Q_S) and longwave (Q_L) flux radiative contributions are negligible over the North Atlantic region (Appendix Figure A1, right).

Given our interest in the Northern Hemisphere we focus primarily on December-January-February (DJF). The ocean heat transport changes in our simulations are also most pronounced during DJF, consistent with the analyses presented in Romanou et al. (2023) and Orbe et al. (2023).

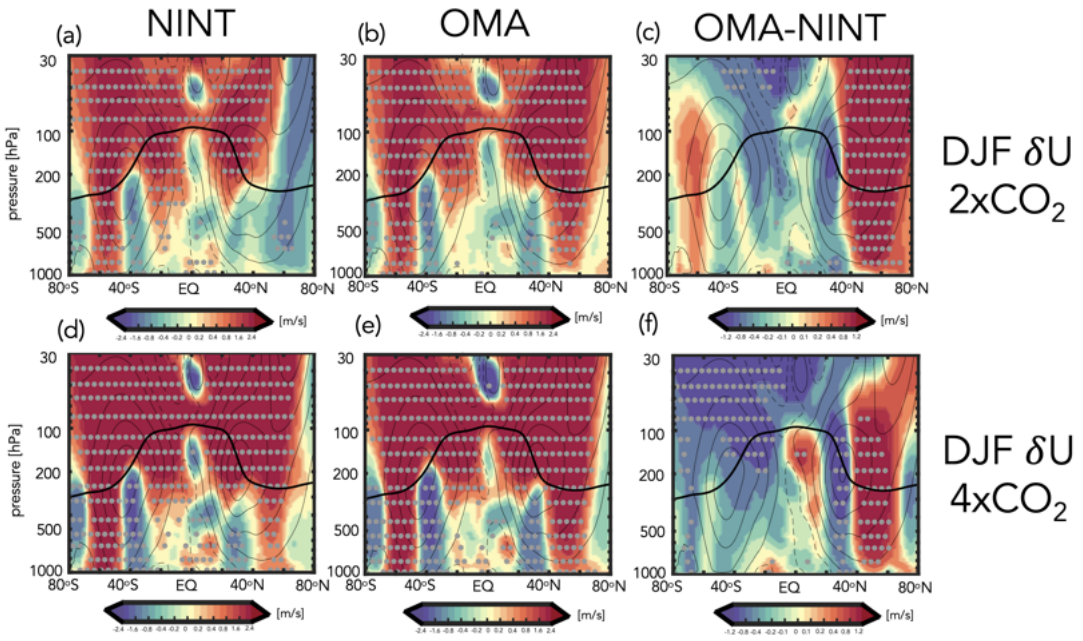

FIG. 1. Colors show the December-January-February (DJF) response of the zonal mean zonal winds, U, to an abrupt doubling (top) and quadrupling (bottom) of CO_2, averaged over years 100-150. Results are shown for NINT (a,d) and fully interactive OMA configurations (b,e), where one ensemble member has been used for each forcing scenario. The OMA - NINT differences are also shown (c,f). Black contours denote climatological mean preindustrial control DJF U values (contour interval: 8 m/s). Stippled regions are statistically significant and the black thick line shows the climatological mean tropopause in the preindustrial control NINT simulation. Note that all colorbar bounds are consistent with those used in Chiodo and Polvani (2019) in order to facilitate comparisons with that study.

3. Results

a. Abrupt 2xCO_2 and 4xCO_2 Zonal Mean Wind Response: OMA versus NINT

Before focusing on ozone feedbacks, we first review the OMA versus NINT differences in NH jet behavior that were presented in Zhang et al. (2023) (Figure 1). In the stratosphere the zonally averaged DJF wind response to 2- and 4xCO_2 features an acceleration at nearly all latitudes, consistent with amplified warming in the tropical upper troposphere (Shaw (2019)) and increased cooling of the stratosphere with height (Garcia and Randel (2008)). Similar wind responses emerge in both the NINT and OMA configurations, except over northern high latitudes at 2xCO_2, where the strengthened zonal winds in NINT are not statistically significant.

In the troposphere, however, there are noticeable differences between the OMA and NINT simulations. In particular, the NH midlatitude jet features a much stronger poleward shift in OMA, compared to NINT (Figures 3 and 6 in Zhang et al. (2023)). As discussed in that study, the stronger response in OMA results in enhanced eddy mixing along isentropes on the poleward flank of the NH jet, resulting in increased transport of tracers from the northern midlatitude surface to the Arctic (not shown). This difference between OMA and NINT occurs at both 2- and at 4xCO_2, resulting in a nonlinearity in the jet (and tracer transport) response in NINT that is not present in the OMA simulations. In the SH, by comparison, the differences between OMA and NINT are much smaller and not statistically significant.

Zhang et al. (2023) hypothesized that the nonlinearity in NH jet behavior evident in the "total" response in the NINT model configuration was related to a nonlinear AMOC response to CO_2 forcing (Figure 2). That is, despite an initial weakening, the AMOC eventually recovers to preindustrial values in the NINT 2xCO_2 simulation, in contrast to the total response to 4xCO_2 in which the AMOC is about 10 SV weaker than the preindustrial control (Fig. 2, left, black box). This results in a so-called "AMOC nonlinearity" to CO_2 forcing of ~-5SV in the NINT configuration. By comparison, in the OMA configuration, the AMOC weakens by ~7 and ~17 SV in the 2- and 4xCO_2 simulations, respectively, representing only a very weak nonlinearity in the long-term response of the AMOC (of ~1.5 SV) (Fig. 2, right, black box).

As it is difficult to meaningfully interpret the zonal mean wind response in the NH, where there are large zonal variations in the midlatitude jet (Simpson et al. (2014)), we next compare the 850 hPa zonal wind changes between the NINT and OMA 4xCO_2 simulations, further distinguishing between "fast" and "total" responses (Figure 3). We begin with the NINT equilibrated or "total" response (i.e. years 100-150), which consists of a poleward jet shift over the Pacific basin and an acceleration and eastward extension of the jet over the Atlantic and Eurasia (Fig. 3b). This pattern is amplified in the OMA run (Fig. 3d), in which both the strengthening and eastward extension of the jet over the Atlantic and its poleward shift over the Pacific are more pronounced. This amplified response in OMA over both the Pacific and Eurasia is also evident at 300 hPa (Appendix Figure A2b).

This wind response in OMA, relative to NINT, is consistent with the jet differences identified in Orbe et al. (2023) between two non-interactive simulations of the GISS low-top climate model in

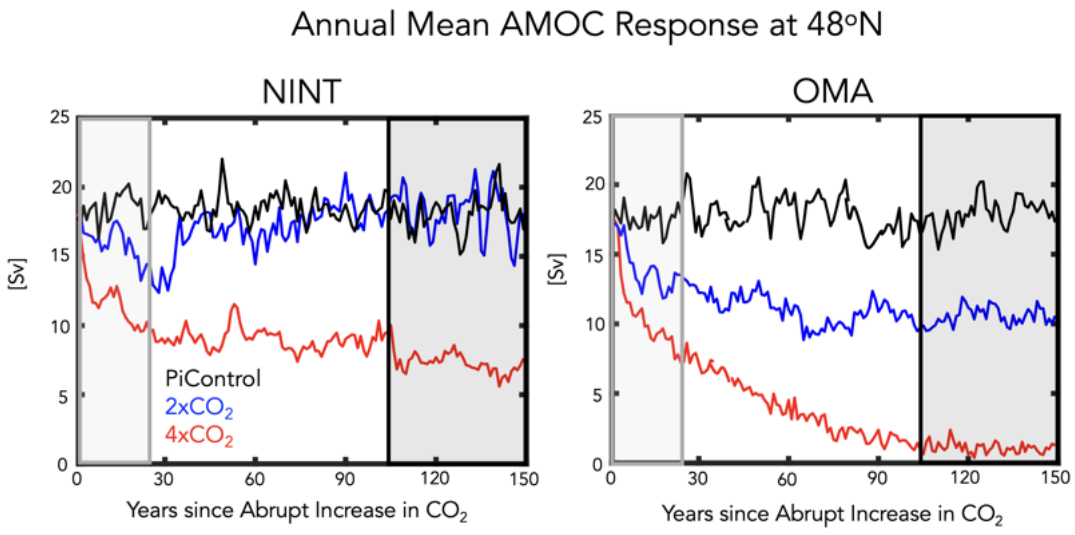

FIG. 2. Evolution of the annual mean maximum overturning stream function in the Atlantic ocean, evaluated at 48°N, for the preindustrial control (black), abrupt $2xCO_2$ (blue) and abrupt $4xCO_2$ (red) simulations. Results for the NINT (left) and OMA (right) configurations are shown. Light grey and black shaded boxes denote the "fast" and "total" timescale response averaging periods.

which only the AMOC strength differed. This suggests that the jet differences between OMA and NINT on these longer timescales are primarily driven by differences in the AMOC response, as hypothesized in Zhang et al. (2023).

Figure 2 (grey boxes) highlights how the AMOC differences between OMA and NINT noted in Zhang et al. (2023) arise very early in the simulations (within the first 20 years). Over these years – which comprise the "fast" response – the impact of interactive chemistry on the zonal wind changes at 850 hPa is very different (Fig. 3a,c). In particular, over the Atlantic, interactive composition results in a strong weakening over the midlatitude jet core and an acceleration on the equatorward flank of the jet (Fig. 3c). This wind change is also evident at 300 hPa (not examined in CP2019), where the winds accelerate on the equatorward and poleward flanks of the midlatitude and subtropical jets, respectively (Fig. A2a). Over the Pacific, where the midlatitude jet is more vertically coherent, interactive chemistry results in an anomalous equatorward jet shift relative to the NINT simulation at both 850 hPa (Fig. 3a) and 300 hPa (Fig. A2a).

This fast composition feedback that occurs over years 5-20 is consistent with the results from CP2019, who showed that the ozone response to $4xCO_2$ induces a weakening of the North Atlantic

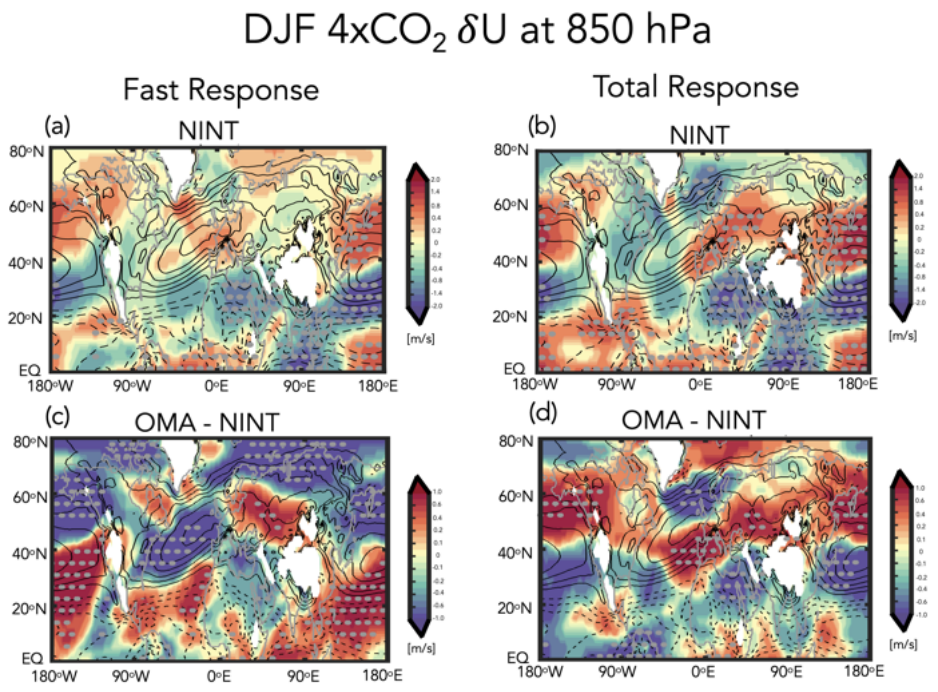

274 FIG. 3. Colors show the 4xCO_2 (four member) ensemble mean change in the DJF 850 hPa zonal winds
275 for the NINT configuration, decomposed into "fast" (i.e. years 5-20) (a) and "total" (i.e. years 100-150) (b)
276 responses. The OMA - NINT fast and total differences are shown in (c) and (d), respectively. Note that one
277 ensemble member is used in displaying the OMA - NINT differences (same as used in Figure 1). Black contours
278 denote climatological mean preindustrial control DJF values (U contour interval: 2 m/s) and stippled regions are
279 statistically significant.

292 jet and a strengthening on its equatorward flank (see their Figure 6). This response is reminiscent
293 of the negative phase of the NAO which previous studies have shown can result in a weaker
294 AMOC (Delworth and Zeng (2016)). In CP2019, however, this response is realized through
295 changes in stratospheric ozone alone, whereas in OMA all trace gases and aerosols are responding.
296 Furthermore, the significance of this rapid response with only one ensemble member is uncertain,
297 particularly during the first 5-20 years when the signal is confounded by large internal variability.
298 To this end, next we present results from the larger (4-member) LINOZ ensemble to examine
299 whether the fast response in the NH jet is related to stratospheric ozone changes.

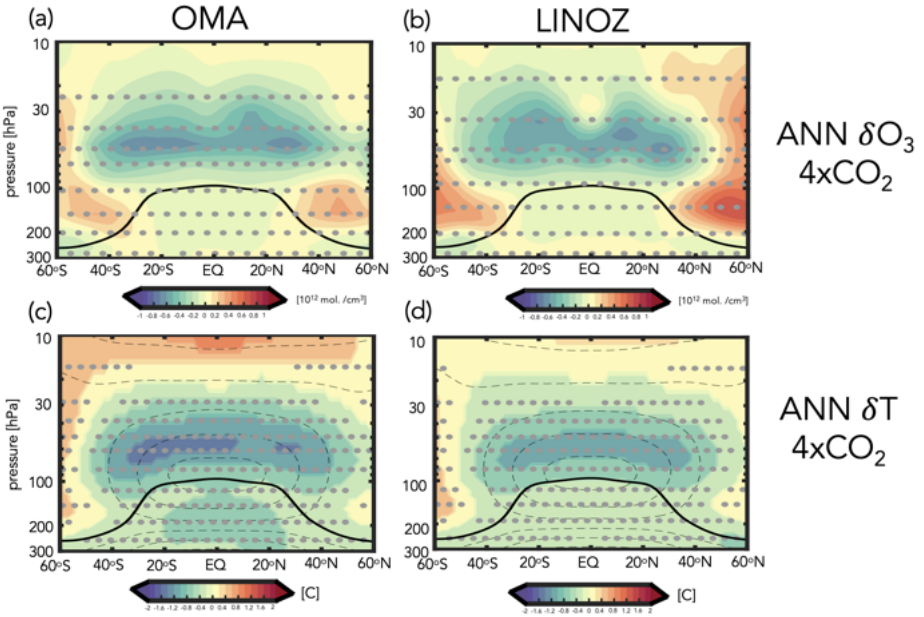

FIG. 4. Colors show the annual averaged change in ozone number density (top) and temperature (bottom) in response to 4xCO_2. Results for OMA (left) and LINOZ (right) are shown, averaged over years 5-20. One simulation is shown for OMA and the four-member ensemble mean response is shown for LINOZ. Black contours in the bottom panels show climatological mean preindustrial control temperatures (contour interval: 10 C). Stippled regions are statistically significant and the black thick line shows the climatological mean tropopause in the preindustrial control NINT simulation.

b. Abrupt 4xCO_2 Stratospheric Ozone and Temperature Responses: OMA versus LINOZ

Before examining the circulation response in the LINOZ ensemble, we first compare the annually averaged ensemble mean LINOZ 4xCO_2 ozone response with that from the OMA simulation (Figure 4). The amplitude and pattern of the ozone response in the LINOZ ensemble (Fig. 4b) is generally very similar to the ozone response in the OMA simulation (Fig. 4a), consistent with Meraner et al. (2020) who showed that the response of ozone to a quadrupling of CO_2 is well captured using linearized schemes. In both OMA and LINOZ configurations the pattern of the 4xCO_2 changes reflects a decrease in tropical LS ozone, associated with enhanced tropical upwelling (Garcia and Randel (2008)), and enhanced concentrations over high latitudes. Over all latitudes the ozone changes are statistically significant, relative to interannual variability in the preindustrial control simulation.

Over northern high latitudes there are some differences in the mid-to-lower stratosphere (~30-100 hPa) between LINOZ and OMA, generally consistent with Chiodo et al. (2018), who found that in this region the ozone response to CO_2 is more dependent on (nonlinear) chemical and transport feedbacks and thus more likely to be captured using a more comprehensive chemistry scheme. Furthermore, both simulations feature small changes in the troposphere. Overall, therefore, the LINOZ scheme captures the gross characteristics of the ozone abrupt 4xCO_2 response expected from previous studies. Note that most of this ozone response occurs in both simulations within the 5-20 years that comprise the "fast" response timescale, as shown in Chiodo et al. (2018) (see their Figure 7b), although full equilibration at high latitudes does take somewhat longer (not shown).

In response to the ozone changes to 4xCO_2 both the OMA simulation and LINOZ ensemble produce cooling in the tropical lower stratosphere and warming over high latitudes (Fig. 4c,d). The amplitude of the cooling is ~3K in the tropical lower stratosphere, and is more-or-less collocated with the region of largest ozone decreases. Further analysis of the temperature tendencies reveals that in our model the cooler temperatures in the tropics (20°S-20°N) and high latitudes (> 40°N) are respectively associated with reduced and increased radiative heating, primarily in the shortwave component (not shown). Dynamically, comparisons of the 4xCO_2 changes in the residual mean stream function show a weaker response in LINOZ, relative to NINT (not shown). This ozone feedback on the Brewer-Dobson circulation, first identified in DallaSanta et al. (2021a), contributes to reduced upwelling, adiabatic cooling, and ozone transport within the lower tropical stratosphere. These circulation changes are therefore not the primary drivers of the temperature response; rather, they are primarily determined by the shortwave radiative response to ozone changes (CP2019).

Despite the somewhat stronger cooling in OMA (Fig. 4c) compared to NINT (Fig. 4d), the temperature response in both configurations is within the 2-4 K range documented in CP2019 (note that all colorbars used are consistent with that study to facilitate comparisons with their results). An important point to note is that the temperature changes due to ozone are of a similar magnitude to the temperature changes due to 4xCO_2 alone in the tropical lower stratosphere (i.e., considering no ozone feedback), where the stratosphere cools by ~2K in the NINT ensemble (not shown). The ozone changes present in LINOZ (and OMA) therefore represent a substantial (~ 50%) feedback on the CO_2-induced cooling in the stratosphere at this altitude.

c. Ozone Feedback on Northern Hemisphere Midlatitude Jet: Fast Response

The temperature response due to ozone is dynamically consequential for the troposphere to the extent that it modifies temperature gradients (and winds) in the lower stratosphere. Indeed, the LINOZ ensemble shows a strong enhancement of lower stratospheric temperature gradients in both hemispheres on both the fast and total response timescales (Fig. 5a,b). In the fast response, this reduction in the meridional temperature gradient near the tropopause has important consequences for the midlatitude jet in both hemispheres, particularly in the NH where it strengthens above and along the jet core and weakens on the poleward flank of the jet over latitudes north of ~ 50°N (Fig. 5c). The winds also accelerate equatorward of the jet core, relative to NINT, in both hemispheres, although the response is only statistically significant in our model in the NH. This ozone-induced response in the jet is very similar to the pattern of the wind response reported in CP2019 (see their Figures 4 and 5). As with the temperature changes occurring in the lower stratosphere, the wind response to ozone changes is similar in magnitude to the $4xCO_2$ response, again suggesting a substantial modulation of the circulation in both hemispheres by ozone changes alone.

The fast zonal mean response to ozone changes reflects a weakening of the midlatitude jet over all longitudes, with the largest negative anomalies concentrated over the Atlantic ocean which are flanked equatorward by positive wind anomalies (Fig. 6a). This LINOZ-NINT wind dipole at 850 hPa is very similar to the fast wind response captured in the fully interactive OMA simulation (Fig. 3c), especially over the Atlantic. This consistency with the response in OMA is also reflected at 300 hPa, where in both LINOZ and OMA configurations the winds accelerate between the climatological subtropical and midlatitude eddy-driven jets (Fig. A2c).

Over the Pacific, by comparison, the OMA and LINOZ responses are different, consistent with CP2019 who also found no robust ozone feedback over that sector (see their Figure 5). This lack of a robust ozone feedback over the Pacific is generally consistent with previous modeling and observational studies showing a much stronger signal of "downward" stratosphere-troposphere coupling over the Atlantic, relative to the Pacific (see Baldwin et al. (2021) and references therein), although this difference between sectors remains speculative and warrants closer inspection beyond the scope of the present study.

In addition to the near surface wind changes, the weakening of the North Atlantic jet in the LINOZ simulations is associated with warming over North America and cooling over the North

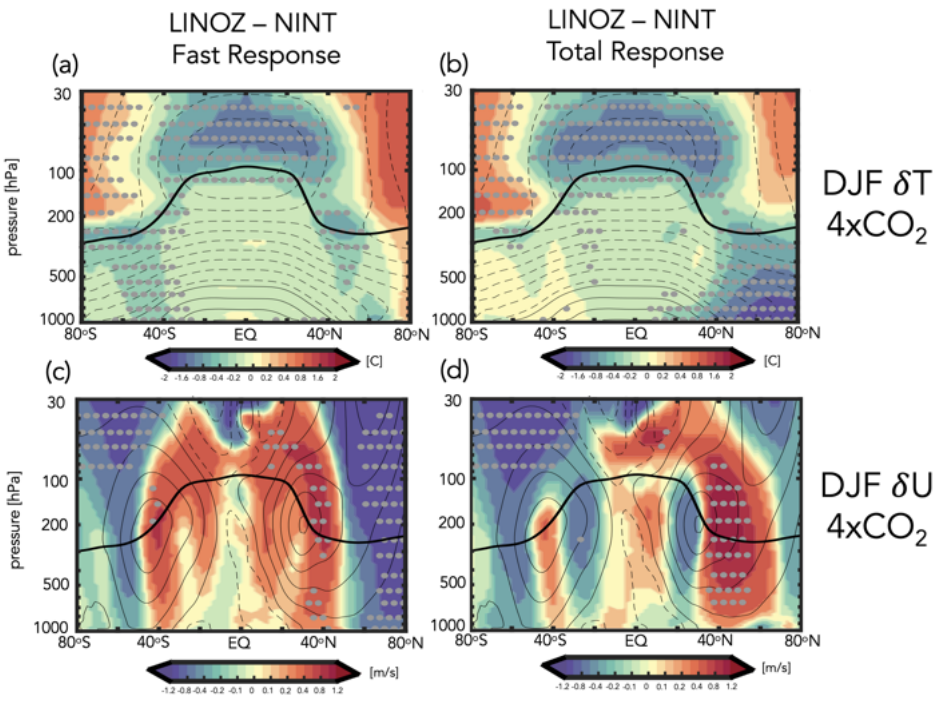

FIG. 5. Colors show the LINOZ-NINT ensemble mean difference in the DJF response of the zonal mean temperatures, T (top) and zonal winds, U (bottom) in response to an abrupt quadrupling of CO_2. Both LINOZ and NINT ensembles consist of four members. Responses are decomposed into "fast" (a,c) and "total" (b,d) changes. Contours denote climatological mean DJF values (T contour interval: 10 C; U contour interval: 8 m/s). Stippled regions are statistically significant and the black thick line shows the climatological mean tropopause in the preindustrial control simulation.

Atlantic and over Eurasia, resembling the negative phase of the NAO (Fig. 6c). A similar surface temperature anomaly was identified in CP2019 (see their Figure 7) and in our model occur in conjunction with positive sea level pressure (SLP) anomalies over the Arctic (Appendix Figure A3, top), both features being reminiscent of a negative NAO.

d. Ozone Feedback on Northern Hemisphere Midlatitude Jet: Total Response

Interestingly, while the fast responses in the winds and temperatures in the LINOZ ensemble are highly consistent with the results from CP2019, our model also simulates a distinct "total" response characterized by strong cooling over the Arctic from the surface to the mid-to-upper troposphere (Fig. 5b). This cooling, which was not identified in CP2019, results in enhanced mid-to-lower

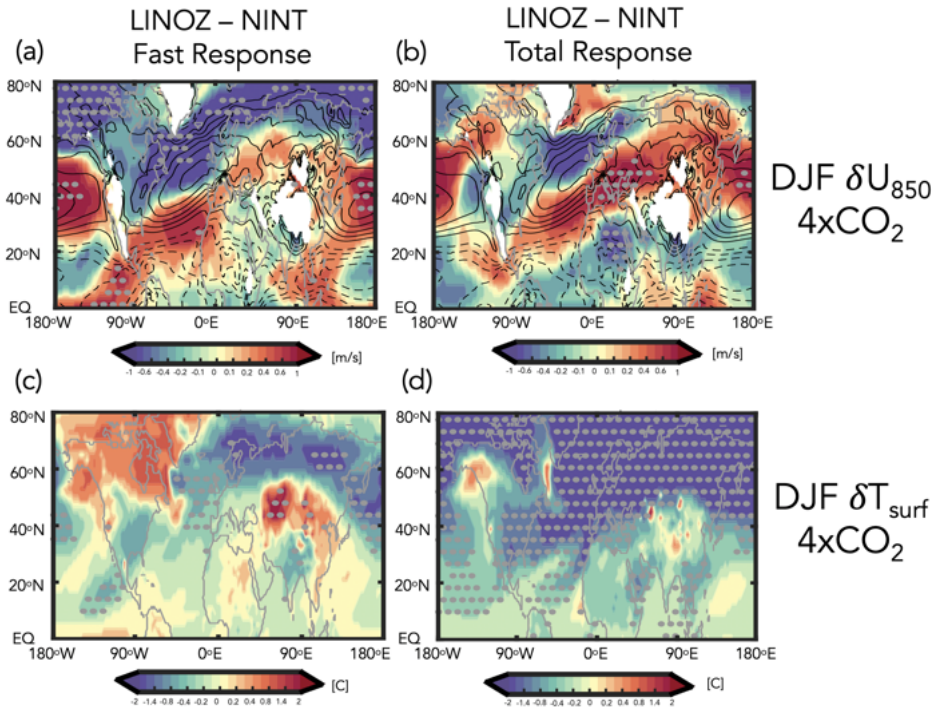

386 FIG. 6. Same as Figure 5, except showing the LINOZ-NINT DJF response in the 850 hPa zonal winds, U_{850}
387 (top) and surface temperatures, T_{surf} (bottom). Contours in top panels denote climatological mean DJF values
388 of U_{850} (contour interval: 2 m/s). Note the similarity between the "fast" wind response shown in (a) and the
389 CP2019 results (their Figure 6).

395 tropospheric temperature gradients, prompting a strong poleward shift of the zonal mean NH jet
396 and a statistically significant acceleration of the winds at 50°N exceeding 2 m/s (Fig. 5d).

397 Zonally, the cooling over the Arctic occurring in the LINOZ ensemble during the total response
398 primarily reflects hemispheric-wide cooling over the Arctic associated with an expansion of the
399 North Atlantic Warming Hole (Fig. 6d). This enhancement of meridional temperature gradients
400 in the lower and mid troposphere drives a poleward shift that spans all longitudes and originates
401 over the North Atlantic (Fig. 6b), where the jet exhibits a distinct acceleration and eastward
402 extension over Europe. Note that over the jet core (40°N-50°N) the winds accelerate (in the zonal
403 mean) during both "fast" (Fig. 5c) and "total" responses (Fig. 5d). However, north of 50°N the
404 responses are very different, with the fast response exhibiting a strong weakening, in contrast to
405 the acceleration ocurring on longer (i.e., "total" response) timescales. This behavior north of 50°N

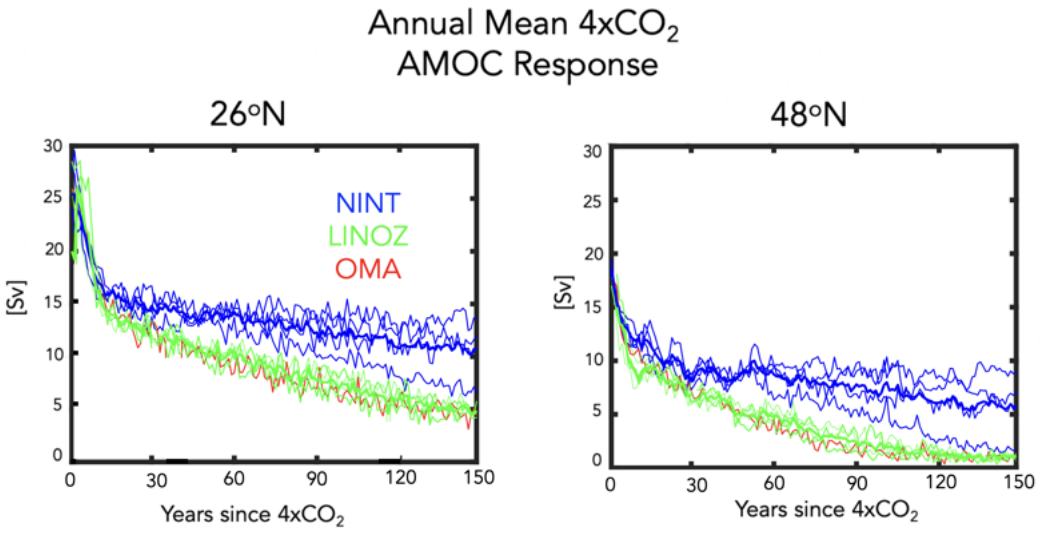

FIG. 7. Evolution of the annual mean maximum overturning stream function in the Atlantic ocean, evaluated at 26°N (left) and 48°N (right) in response to $4xCO_2$. Results for the LINOZ and NINT ensembles are shown in green and blue, respectively (thick lines denote ensemble means). Red lines show the response in the OMA simulation.

was not captured in CP2019 and comprises a coupled ozone-ocean feedback that is distinct from what was outlined in that study.

e. Total Ozone Feedback: Modulation by the AMOC

The "total" responses in the tropospheric winds and temperatures that occur in the LINOZ ensemble are not obviously linked to ozone-driven temperature changes in the stratosphere, which do not extend into the troposphere. What, then, is the driver of the lower tropospheric high latitude cooling, if it is not directly linked to ozone-driven stratospheric temperature changes?

As expected from the OMA and NINT results presented in Zhang et al. (2023) and summarized in Figure 2, we find that the strong cooling that occurs over the NH in the total LINOZ response is also related to a weakening of the AMOC at $4xCO_2$ (Mitevski et al. (2021); Orbe et al. (2023)). In particular, Figure 7 shows stronger weakening of the AMOC in the LINOZ (green lines) ensemble, relative to NINT (blue lines) at both 26°N (left) and at 48°N (right). Despite large internal variability, the LINOZ ensemble shows a more rapid decline of the AMOC, a difference that is evident at both latitudes.

Interestingly, comparisons of the AMOC behavior in LINOZ with the fully interactive OMA simulation (red line) shows a striking similarity (and the mechanism of these changes is also similar, as shown in Section 3f). This similarity is surprising, given that other (non-ozone) trace gases and aerosols are also evolving in the OMA experiment. In particular, Rind et al. (2018), using a previous version of the model, observed an indirect effect of natural aerosols (primarily sea salt) on AMOC stability. They showed that aerosols enhanced the local cooling of SSTs in regions of increased cloud cover in a warmer climate by acting as condensation nuclei and thereby raising cloud optical thickness and ocean surface cooling. This surface cooling was then linked to reduced evaporation relative to precipitation, resulting in anomalously positive surface freshwater forcing and reduced North Atlantic Deep Water (NADW) production. That study, however, focused on aerosol-induced AMOC cessations occurring on multicentennial timescales long after the initial (abrupt) warming. By comparison, the results in Figure 7 identify an impact of ozone on the AMOC that occurs within the first 20 years of the initial CO_2 forcing – that is, over the period during which ozone is also rapidly evolving (Chiodo et al. 2018) and stratospheric temperature gradients are most impacted by changes in ozone (not aerosols). Our results, therefore, highlight that during this time frame the AMOC can be as (if not more) sensitive to wind-driven buoyancy changes forced by stratospheric ozone anomalies as they are to aerosol-induced changes in freshwater forcing.

Before elucidating the mechanism of the AMOC changes in the LINOZ ensemble, we first identify the region over which the largest differences in mixed layer depth begin to emerge between the LINOZ (OMA) and NINT simulations. In particular, the weaker AMOC in the LINOZ and OMA runs is found to be accompanied by a rapid reduction in mixed layer depths, which occur primarily in the Irminger Sea region (55°N-65°N, 40°W-20°W) (Figure 8). The mixed layer depth differences among the configurations in the Labrador Sea are, by comparison, negligible. East of the Irminger Sea (i.e., 55°N−65°N, 20°W-0°) we also identify differences between the ensembles (not shown), but these emerge later, suggesting that the Irminger Sea changes are likely the initiators of the differences in AMOC behavior between the NINT and LINOZ ensembles. The same region was identified in Romanou et al. (2023) as being key for determining the sensitivity of the AMOC in various SSP 2-4.5 ensemble runs, albeit for simulations conducted using the low-top GISS climate model.

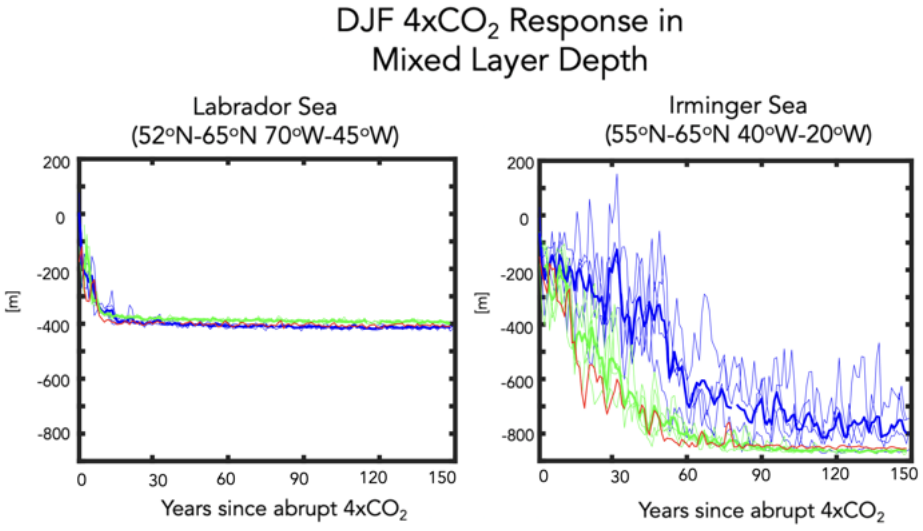

FIG. 8. Changes in the DJF mixed layer depths, evaluated over the Labrador Sea (left) and Irminger Sea (right) in response to $4xCO_2$, relative to the preindustrial control simulations. Results for the LINOZ and NINT ensembles are shown in green and blue, respectively (thick lines denote ensemble means). Red lines show the response in the OMA simulation.

f. Ozone Feedback Dependence on the AMOC: Linking Fast and Total Responses

Is the fact that the AMOC declines more rapidly in the LINOZ ensemble – and the OMA simulation – a response to the ozone changes in those simulations or just a coincidence? In the fast response the zonal wind changes over the North Atlantic reflect a weakening of the jet core that is flanked equatorward by positive anomalies, resembling a negative NAO pattern. Indeed, a negative (positive) NAO has been associated with a weaker (stronger) AMOC by adding (extracting) heat to/from the subpolar gyre, resulting in reduced (increased) NADW formation (Delworth and Zeng (2016)). Here we argue that such a mechanism is present in our model simulations, resulting in a long-term modulation of the NH midlatitude jet by ozone that occurs indirectly through changes in the AMOC.

In particular, Figure 9 shows maps of the surface zonal wind, surface friction speed, mixed layer depth, net heat fluxes, sea surface temperatures, and north-south heat and salinity ocean transports, averaged over years 1-5. In response to an abrupt quadrupling of CO_2, the surface winds weaken over the subpolar North Atlantic region in NINT, leading to a weak acceleration of the zonal winds

on the poleward flank of the North Atlantic jet (~60°N-70°N) (Fig. 9a, top). Over the subpolar North Atlantic the weakening of the surface winds leads to a significant reduction in surface friction speed (Fig. 9b, top) and mixed layer depths (Fig. 9c, top), as well as increased heat flux into the ocean (in the form of reduced latent heat fluxes out of the ocean) (Fig. 9d, top) and warmer sea surface temperatures (Fig. 9e, top). The reduced surface density during the first 20 years associated with these warmer temperatures lead to a rapid decrease in mixed layer depth by some 200 m (Figure 8) and the overturning circulation by ~ 40% (Figure 7) in NINT. At these early years the changes in meridional heat and salinity transports over the Irminger Sea are relatively small (Fig. 9fg, top).

However, in response to the ozone changes captured in the LINOZ ensemble during years 1-5, there is an even stronger reduction in the surface zonal winds and friction speed (Fig. 9 ab, bottom), consistent with the negative NAO response evident in the 850 hPa zonal winds (Fig. 6c, top). The surface friction changes align closely with the reduced mixed layer depths which extend well into the Irminger Sea region and over latitudes further south of the subpolar gyre (Fig. 9c, bottom).

The reductions in mixed layer depth that occur over the Irminger Sea are likely driven by the reductions in surface wind speed which increase (primarily latent) heat fluxes into the ocean (Fig. 9d, bottom), driving warmer sea surface temperatures in LINOZ, relative to NINT (Fig. 9e, bottom). The sign of the response of the heat fluxes in the subpolar gyre region is consistent with previous studies showing that a positive (negative) phase of the NAO implies reduced (enhanced) atmosphere to ocean heat fluxes (Delworth et al. (2017)). Furthermore, the spatial pattern of the heat flux response is very similar to the NAO heat flux composites that were prescribed in Delworth and Zeng (2016) and inferred from observations in Ma et al. (2020) (see their Figure 6), who showed that there is much greater heat loss from the ocean over the subpolar region in association with a jet strengthening.

At the same time, the changes in freshwater forcing (P-E) during this time period are negligible such that the net buoyancy forcing comprising the sum of both net heat and freshwater fluxes (~Q+F) is positive. This stabilizing buoyancy forcing from surface warming makes the mixed layer depths shallower by suppressing convective mixing, shutting down NADW production (Alexander et al. (2000); Kantha and Clayson (2000)). There is also an initial change in the north-south heat and salt transports that is colocated with the dipole anomaly in the surface friction speed, promoting

anomalous poleward salt and heat transport into the subpolar gyre (Fig. 9fg, bottom). This feature is confined to the top few ocean layers (not shown) and the implied anomalous heat transport could be contributing to the warmer sea surface temperatures in that region, in addition to the surface heat flux changes.

Over the ensuing years (5-20) a similar pattern is maintained in the LINOZ ensemble (Figure 10, middle row). The reduction in NADW, however, results in reduced northward heat and salinity transports (Fig. 10 fg, middle) throughout the ocean columm. While this results in cooler SSTs south of the subpolar gyre region (Fig. 10e, middle), which otherwise might enhance the density of the near-surface water masses, the reduced northward salinity transports prevent the AMOC from restarting. Interestingly, the results from the OMA simulation show a very similar response as the LINOZ ensemble (Figure 10, bottom row), suggesting that stratospheric ozone changes in that simulation are also likely the primary driver of the weaker AMOC in that model configuration. This sequence of processes linking the surface wind changes to anomalous heat fluxes and reduced NADW is basically identical to what is outlined in Figure 4 of Delworth and Zeng (2016) and Figure 1 of Khatri et al. (2022). Additional analysis of the 2xCO_2 simulations, which feature a stronger AMOC decline in OMA (and LINOZ) compared to NINT (Figure 2), reveals that a similar mechanism for reduced NADW production occurs at lower CO_2 forcing (not shown).

Examining the timescale of the responses of the variables shown in Figures 9 and 10 reinforces the strong coupling between the changes in surface friction speed, sea surface temperature, latent heat fluxes and mixed layer depth changes over the Irminger Sea region (Figure 11a-d). Despite large internal variability, there is a clear separation between the LINOZ (and OMA) and NINT ensembles that emerges around year 15 (black dashed lines). The changes in sensible heat emerge after the latent heat fluxes (Fig. 11e), suggesting that the latter play a more important role in initializing the heat flux differences in LINOZ (and OMA), relative to NINT.

Finally, while they may contribute to enhanced positive buoyancy forcing later in the integrations, the freshwater forcing anomalies (F = P-E) are shown to be negligible during the initial years following the abrupt quadrupling of CO_2 (Fig. 11f), indicating that the primary driver of the initial difference between the LINOZ (and OMA) and NINT runs is related to the surface wind-driven changes as they impact the latent heat fluxes into the ocean. This is consistent with Roach et al. (2022) who showed a much stronger correlation between AMOC strength at 26°N and the

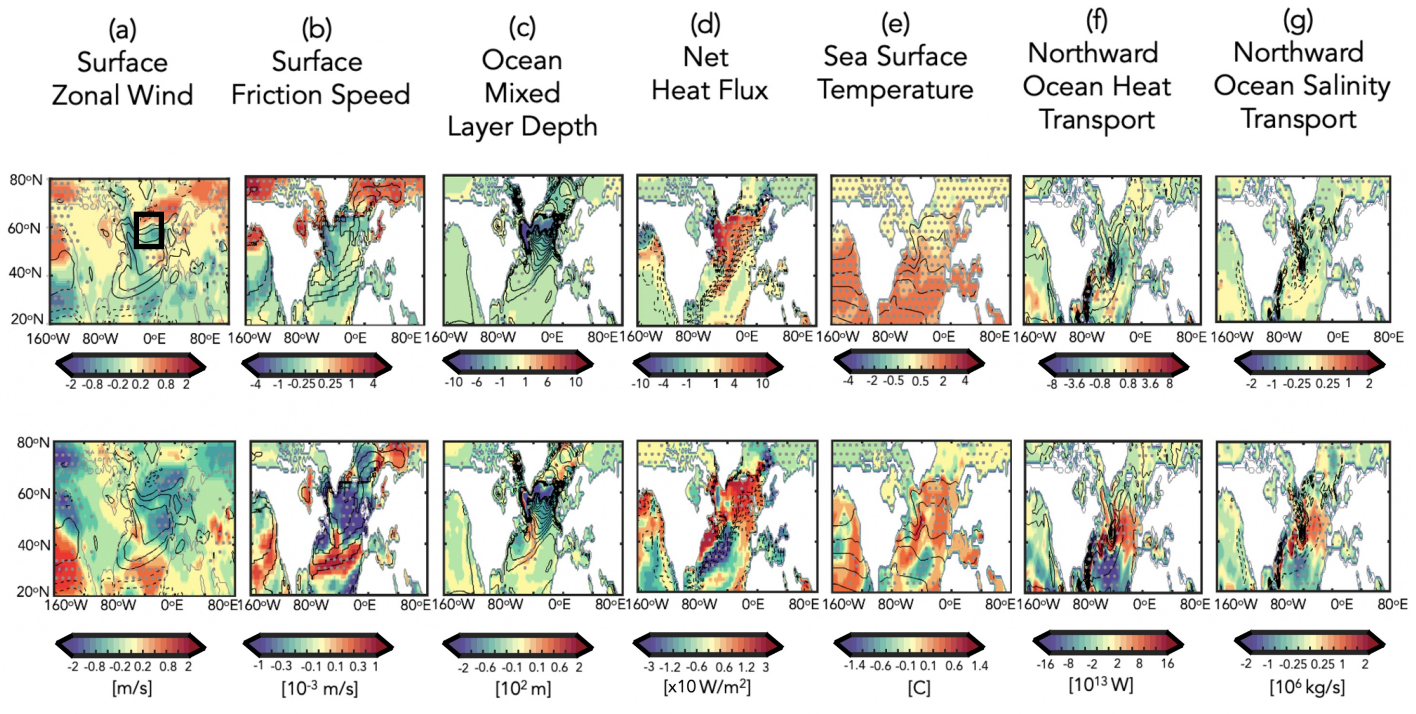

505 FIG. 9. Top panels: Colors show the December-January-February (DJF) response of the surface zonal wind (a), surface friction speed (b), ocean
506 mixed layer depth (c), net heat flux (sum of sensible plus latent heat) (d), sea surface temperature (e) and northward heat (f) and salt (g) transports in
507 response to an abrupt quadrupling of CO_2. Results are shown for the 4-member ensemble averaged NINT configuration. Bottom panels: Same as top
508 panels, except showing the LINOZ minus NINT ensemble mean difference. For both top and bottom panels, responses have been averaged over years
509 1-5 since "branching" from the preindustrial control simulation. Stippled regions are statistically significant and black contours denote climatological
510 mean preindustrial control DJF values. Contour intervals: surface zonal wind [2 m/s], surface friction speed [2.5x10^{-3} m/s], mixed layer depth [60 m],
511 net heat flux [30 W/m^2], sea surface temperature interval [2 C], northward heat flux [2x10^{12} W], and northward salt flux [10^6 kg/s]. The black box in
512 (a) bounds the Irminger Sea region over which the spatial averages in Figure 8b and Figure 11 are evaluated.

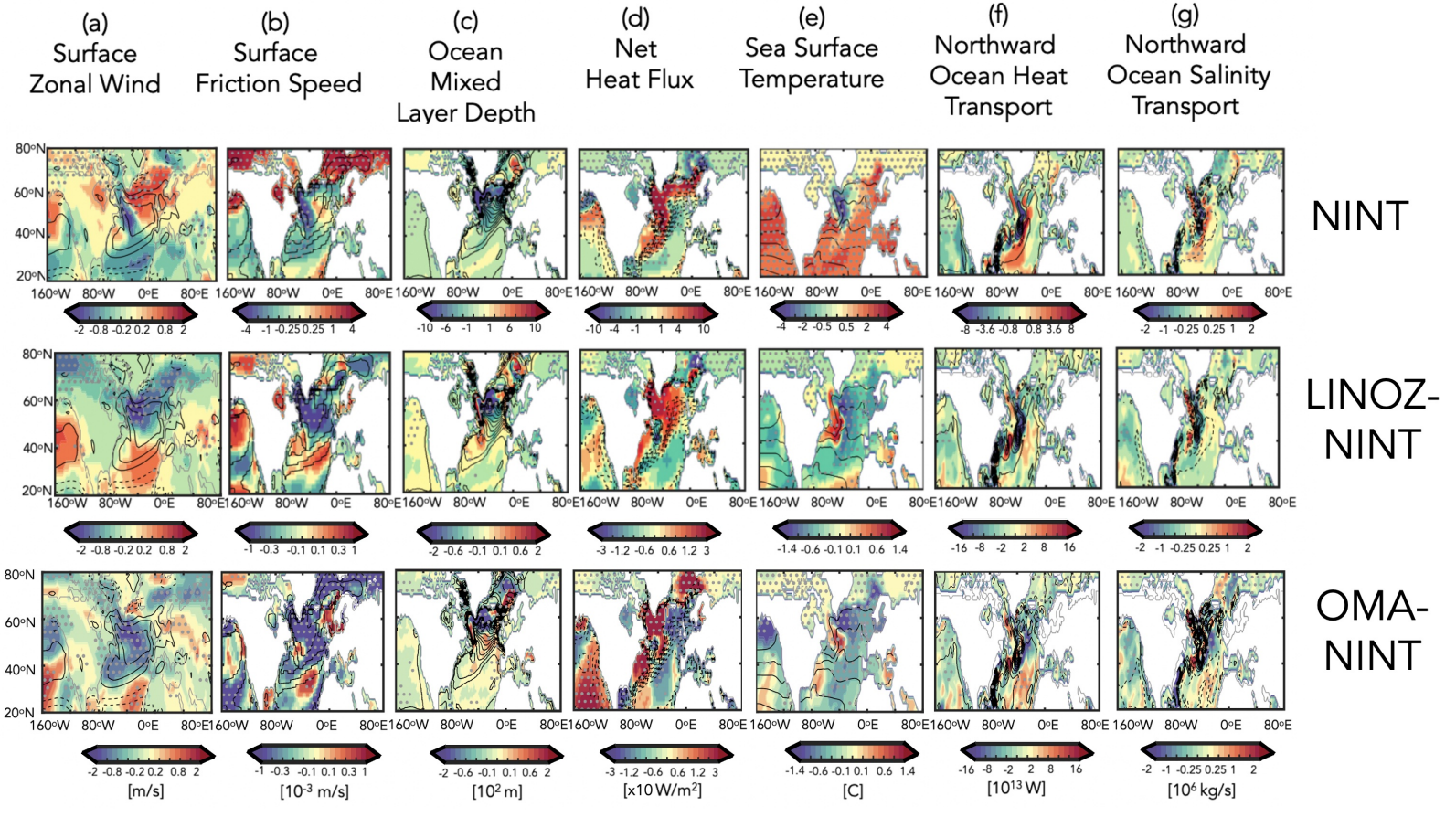

526 FIG. 10. Same as Figure 9, except showing the responses, averaged over years 5-20. An extra row at the bottom has been added, showing the OMA -
527 NINT differences, where the ensemble members shown in Figures 1, 2 and 3 have been used. Same contour intervals and colorbars have been used as
528 in Fig. 9.

heat component of the surface buoyancy flux, relative to the freshwater component, in various experiments using the Community Earth System Model version 1 (CESM1) in which the winds over the subpolar gyre were nudged to reanalysis values. Note that in our model other potential contributors to freshwater forcing from sea ice do reveal differences between the LINOZ, OMA and NINT ensembles, but these emerge several years (i.e., years ~20-30) after the changes in sea surface temperatures and heat fluxes (not shown).

g. Ozone Driver of AMOC Changes: Fixed SST and SIC Results

So far, we have shown that the stratospheric ozone changes that occur in response to 4xCO_2 result in a negative NAO response over the North Atlantic (Fig. 5,6). In our model this triggers a more rapid decline of the AMOC (Fig. 7) through surface-wind driven changes in heat fluxes into the ocean (Fig. 9,10). While the time series analysis (Fig. 11) reveals that the AMOC changes in the LINOZ (OMA) ensemble occur on similar timescales as the wind (and heat flux) changes, one potentially confounding factor is the fact that the AMOC reduction itself results in reduced wind speeds over the subpolar gyre region. These reduced near-surface winds are associated with an anomalous anticyclonic flow pattern (Fig. A3, top; also discussed in Gervais et al. (2019); Romanou et al. (2023); Orbe et al. (2023)), which could contribute to the reduced heat fluxes and subsequent changes in NADW production. Therefore, to more convincingly link the surface wind speed changes to the stratospheric ozone changes aloft, we next examine results from the fixed preindustrial control SST and SIC experiments.

Figure 12 shows the ozone-induced zonal wind and temperature changes averaged over the last twenty years of the fixed preindustrial control SST and SIC experiments in which the time-varying zonally varying ozone from the 4xCO_2 LINOZ ensemble is prescribed (Fig. 12 a,b). Recall that in the fixed SST and SIC experiments, only the ozone evolution differs from the preindustrial control simulation, as CO_2, SSTs and SIC are all set to preindustrial values. Comparisons with results from the fully coupled LINOZ "fast" response (see Fig. 5a,c) reveal a very similar picture. This similarity between the fully coupled fast response and the fixed preindustrial control SST and SIC experiments is striking, both featuring a similar change in the NH jet associated with enhanced temperature gradients in the lower stratosphere as first reported in CP2019.

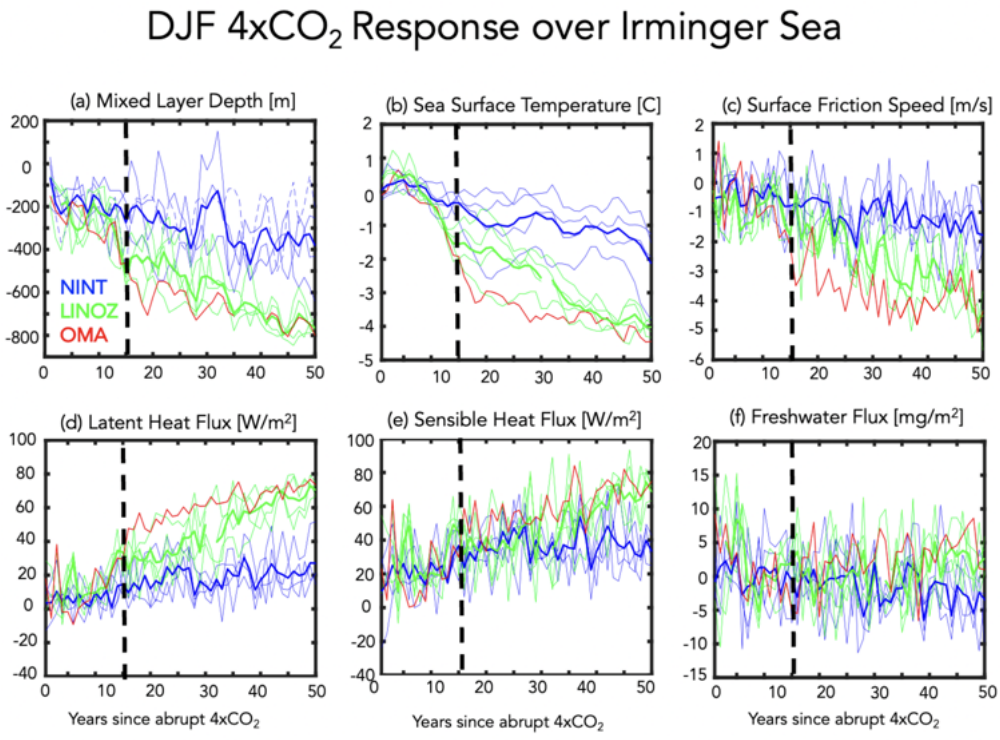

548 FIG. 11. Changes in the DJF mixed layer depths (a), sea surface temperatures (b), surface friction speed (c),
549 latent heat fluxes (d), sensible heat fluxes (e) and precipitation minus evaporation (f) in response to 4xCO_2,
550 relative to the preindustrial control simulations. Averages are performed over the Irminger Sea (55°N-65°N,
551 40°W-20°W) and the x-axis is restricted to years 1-50 in order to highlight the fast timescales on which the mixed
552 layer depths, surface friction speed and heat fluxes evolve together. Results for the LINOZ and NINT ensembles
553 are shown in green and blue, respectively (thick lines denote ensemble means). Red lines show the response in
554 the OMA simulation. Black vertical lines indicate year ~15 at which point the mixed layer depth responses in
555 the LINOZ and NINT ensembles diverge. Note that the freshwater flux unit of 1 mg/m^2 per second (≡ 0.0864
556 mm/day ≡ 3.1 cm/year) is used, because at 5°C it contributes approximately the same ocean density flux as the
557 heat flux unit of 1 W/m^2 (Large and Yeager (2009)).

580 Comparisons of the 850 hPa zonal winds and surface temperatures over the North Atlantic
581 (Fig. 12c,d) also reveal a strikingly similar response between the fully coupled ensemble and the
582 fixed preindustrial control SST and SIC experiments (compare with Fig. 6a,c). Over the Atlantic
583 this similarity also holds aloft in the zonal wind response at 300 hPa (Fig. A2e) and in the sea
584 level pressure response (Fig. A3, bottom). The consistency in the sea level pressure changes is

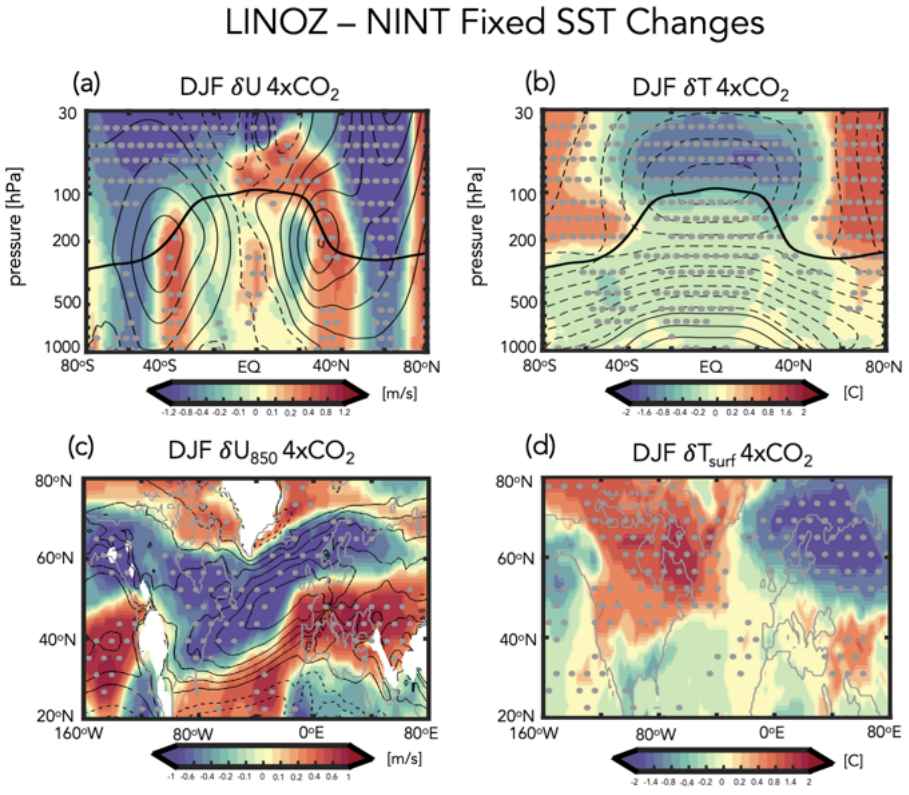

590 FIG. 12. Top panels: Colors show the 4xCO_2 ensemble mean response in zonal mean zonal winds, U (a),
591 temperatures, T (b), 850 hPa zonal winds, U_{850} (c) and surface temperature, T_{surf} (d) in the prescribed SST and
592 SIC experiments in which the time-evolving 4xCO_2 ensemble mean LINOZ ozone response is prescribed. Note
593 that SSTs, SICs and background CO_2 are all set to preindustrial values. Averages are shown over the last 20 years
594 (years 40-60) of the integrations. Black contours, where shown, denote climatological mean preindustrial control
595 DJF values (U contour interval: 8 m/s; T contour interval: 10 C; U_{850} contour interval: 2 m/s). Stippled regions
596 are statistically significant and the black thick line in the top panels shows the climatological mean tropopause in
597 the preindustrial control simulation.

585 interesting as it suggests that over the North Atlantic stratospheric ozone changes alone can result
586 in a significant reduction in the near surface winds that is on the same order (if not larger than)
587 the 4xCO_2 response. In our coupled atmosphere-ocean model this additionally results in heat
588 flux changes that are large enough to reduce NADW production, resulting in a significant (i.e.
589 ~30-40%) long-term change in AMOC strength.

4. Conclusions

Here we have used the NASA GISS coupled atmosphere-ocean high-top model (E2.2-G) to examine how coupled changes in stratospheric ozone and the ocean circulation both influence the abrupt 4xCO_2 response of the NH midlatitude jet. Our key results are as follows:

- The NH midlatitude jet response to 4xCO_2 is modulated by coupled feedbacks from both stratospheric ozone and the AMOC, which occur on "fast" (5-20 year) and "total" (100-150 year) timescales, respectively.

- In the "fast" response, the zonal mean jet weakens (strengthens) on its poleward (equatorward) flank, consistent with reduced LS temperature gradients associated with ozone loss in the tropics. Zonally, this jet change is expressed as a negative NAO-like pattern, consisting of weaker zonal surface winds over the North Atlantic, consistent with the findings in CP2019.

- The weaker winds over the North Atlantic are associated with increased (primarily latent) heat fluxes into the ocean, which initially result in warmer SSTs over the subpolar gyre region, reducing NADW production and leading to more rapid weakening of the AMOC.

- A reduced AMOC leads to widespread cooling over the Arctic which enhance mid-to-lower tropospheric temperature gradients, resulting in a poleward shift of the NH midlatitude jet. This "total" response is consistent with previous studies showing that a weakening of the AMOC results in a stronger and poleward shifted jet in the NH (e.g., Bellomo et al. (2021); Orbe et al. (2023); Liu et al. (2020); Zhang et al. (2023)).

Taken together, the findings listed above indicate that the stratospheric ozone feedback on the NH midlatitude jet reported in CP2019 is coupled to the behavior of the AMOC during the "fast" response, wherein the jet weakens over the North Atlantic. In our model, this wind response extends to the surface, resulting in reduced heat fluxes out of the subpolar gyre region and a more rapid decline of the AMOC. On longer timescales, these changes in the AMOC subsequently drive a poleward shift in the NH midlatitude jet. Unlike the "fast" response, this "total" timescale response in the NH jet to changes in stratospheric ozone has not been previously reported, to the best of our knowledge. This may reflect differing sensitivities of the AMOC among models and our results will, of course, need to be tested using other models to assess robustness.

Another intriguing result from this study is that the stronger decline of the AMOC in the LINOZ ensemble does not appear to be a coincidence. Rather, in our model, the "fast" ozone and "total" AMOC feedbacks on the NH jet are coupled through surface-wind driven changes in heat fluxes into the ocean. Key here is the fact that this sensitivity in the AMOC is driven only by changes in stratospheric ozone, which we have isolated from changes in other trace gases and aerosols. Thus, while previous studies (Rind et al. (2018)) have identified an important influence of interactive composition on the AMOC, they have mainly implicated the indirect effect of aerosols on clouds through changes in sea surface temperatures and how these impact P-E (and net surface freshwater forcing). To the best of our knowledge, no study has previously demonstrated an impact of stratospheric ozone changes alone on the AMOC response to a quadrupling of CO_2. Despite the different mechanisms at play, however, are results are generally consistent with those from Rind et al. (2018) in highlighting the need for renewed focus on surface flux observations to help assess overturning stability.

An important caveat with our results is related to known biases in vertical mixing and NADW production in the ocean component of the GISS model (Miller et al. (2021); Romanou et al. (2023)) which likely explain why the low-top version of the coupled atmosphere-ocean climate model (E2.1-G) exhibits a more sensitive AMOC response to a quadrupling of CO_2, compared to some other models (Bellomo et al. (2021)). An important point to highlight, however, is that the high-top model employed in this study is much less sensitive, as the AMOC weakens by ~10 SV in response to 4xCO_2, compared to a complete collapse in E2.1-G (see Figure 31 in Rind et al. (2020)). That study showed that this may be related to differences in the parameterization of rainfall evaporation associated with moist convective precipitation, which they show has a strong influence on the AMOC sensitivity in the GISS model via its effect on moisture loading in the atmosphere. While an exhaustive comparison between the models is beyond the scope of this study, the relevant point here is that the 4xCO_2 AMOC response simulated in the E2.2-G NINT ensemble is well within the CMIP5 and CMIP6 ranges documented in Mitevski et al. (2021) (see their Supplementary Figure S3).

A natural next step for future research is to examine whether this influence from stratospheric ozone is evident in more realistic scenarios. Although not examined in equal depth, results from the more realistic 1%CO_2 transient simulations also show a greater weakening of the AMOC in OMA,

relative to NINT, indicating that the findings presented here are not an artifact of the abruptness of the forcing (not shown). Analysis of the more comprehensive historical and future Shared Socioeconomic Pathway (SSP) (Meinshausen et al. (2020)) integrations is currently underway to identify other factors, including aerosols and the solar cycle (Muthers et al. (2016)), which are likely to influence the ocean circulation. For sake of brevity, however, we reserve further discussion of the more comprehensive results for future work.

Finally, our results linking the fast timescale jet response to the ensuing AMOC changes underscore the profound impact that changes in lower stratospheric winds alone can have on surface climate, as highlighted in Sigmond and Scinocca (2010). Quite remarkably, our fixed SST and SIC experiments showed that these lower stratospheric wind changes are driven primarily by changes in ozone and not by background changes in CO_2 or in sea surface boundary conditions. Taken together, our results suggest that more attention needs to be paid to understanding the time-evolving response of the coupled Earth system to future ozone changes, with a focus on changes in ocean heat transport and how these feed back on the NH jet stream.

Acknowledgments. C.O. acknowledges helpful discussions with Lettie Roach, Ivan Mitevski and Lorenzo Polvani. G.C. acknowledges support by the SNSF with the "Ambizione" grant N. PZ00P2180043. Climate modeling at GISS is supported by the NASA Modeling, Analysis and Prediction program, and resources supporting this work were provided by the NASA High-End Computing (HEC) Program through the NASA Center for Climate Simulation (NCCS) at Goddard Space Flight Center.

Data availability statement. The NINT and OMA GISS E2.2-G simulations used in the study are available at the CMIP6 archive via the Earth System Grid Federation (`https://esgf-node.llnl.gov/`), where NINT and OMA are respectively denoted as "physics version 1" and "physics version 3". The specific simulations used here are the PiControl, abrupt-2xCO_2, and abrupt-4xCO_2 r1i1p1f1 (NINT) and r1i1p3f1 (OMA) runs. Output needed to reproduce all figures showing the additional three NINT 4xCO_2 simulations, fixed SST simulations as well the four-member LINOZ ensemble is available online at `https://gmao.gsfc.nasa.gov/gmaoftp/corbe/AMOC_Linoz/Data/`. All GISS ModelE components are open source and available at http://www.giss.nasa.gov/tools/modelE/.

APPENDIX

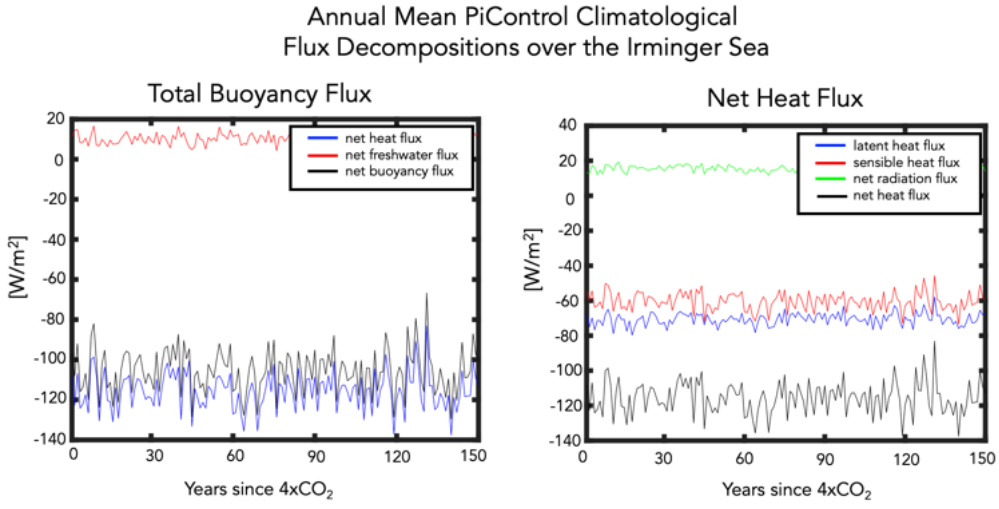

FIG. A1. Left: Decomposition of the net surface buoyancy flux (black) into contributions from net heat (blue) and net freshwater (red) fluxes. Right: Further decomposition of the net surface heat flux (black) into contributions from latent heat fluxes (Q_E (blue)), sensible heat fluxes (Q_H (red)), and combined solar and longwave radiative fluxes (Q_S+Q_L (green)). Results are shown for 150 years of the NINT preindustrial control (PiControl) simulation, evaluated over the Irminger Sea.

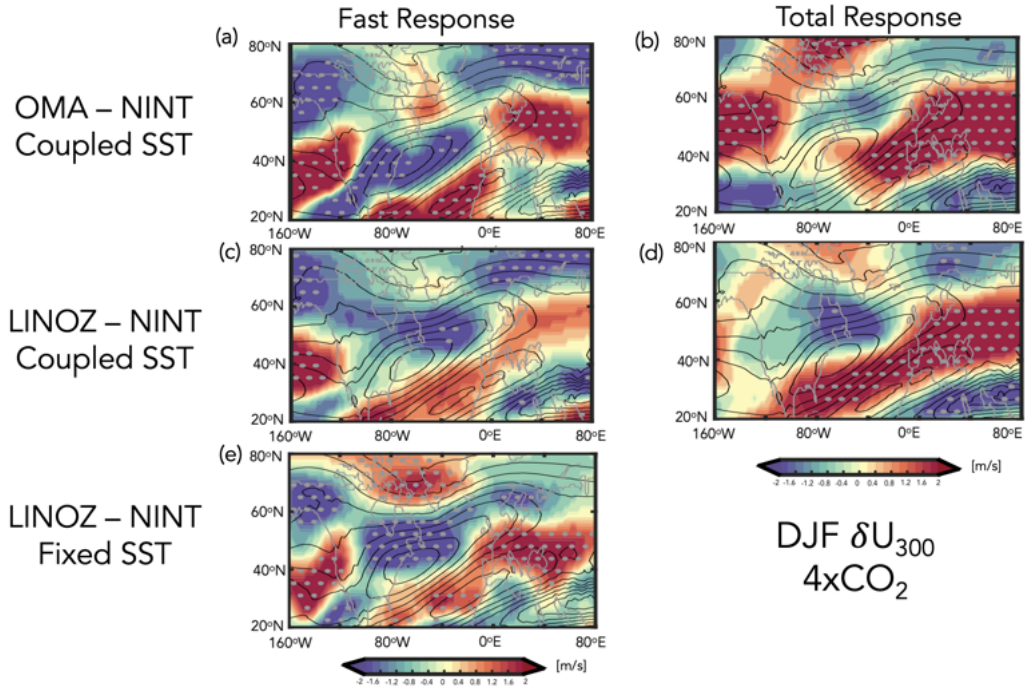

691 FIG. A2. Colors show the coupled atmosphere-ocean OMA - NINT (a,b) and LINOZ - NINT (c,d) $4xCO_2$
692 changes in the DJF 300 hPa zonal winds. One ensemble member is used in the top panels, compared to four
693 members in the middle row. Panel e shows results from the atmosphere-only ensemble in which the time-evolving
694 $4xCO_2$ ensemble mean LINOZ ozone response is prescribed and the SSTs, SICs, and background CO_2 are set to
695 preindustrial values. Left and right panels in the top and middle rows show the responses decomposed into "fast"
696 (i.e. years 5-20) (a,c) and "total" (i.e. years 100-150) (b,d) responses. Averages over years 40-60 are shown
697 for the prescribed SST and SIC experiments in panel e, which equilibrate much more rapidly, compared to the
698 coupled experiments. Black contours denote climatological mean preindustrial control DJF values (U contour
699 interval: 2 m/s) and stippled regions are statistically significant.

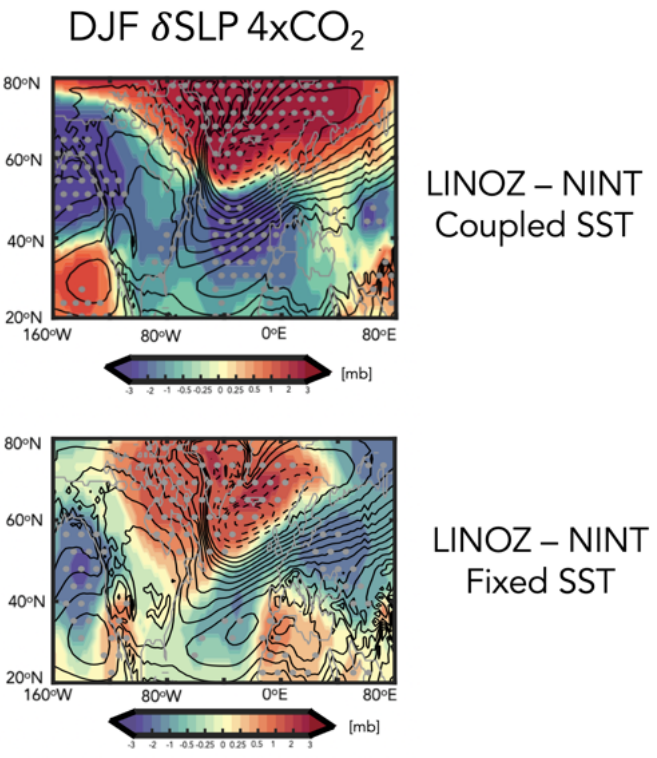

FIG. A3. Top panel: Colors show the LINOZ minus NINT ensemble mean difference in the December-January-February (DJF) "fast" response of the sea level pressure to an abrupt quadrupling of CO_2. Results are shown for the fully coupled atmosphere-ocean simulations. Bottom panel: The ensemble mean response in sea level pressure in the experiments in which the time-evolving 4xCO_2 ensemble mean LINOZ ozone response is prescribed and the SSTs, SICs, and background CO_2 are set to preindustrial values. Black contours denote climatological mean preindustrial control DJF values (contour interval: 10 mb). Stippled regions are statistically significant.

References

Alexander, M. A., J. D. Scott, and C. Deser, 2000: Processes that influence sea surface temperature and ocean mixed layer depth variability in a coupled model. *Journal of Geophysical Research: Oceans*, **105 (C7)**, 16 823–16 842.

Ayarzagüena, B., and Coauthors, 2020: Uncertainty in the response of sudden stratospheric warmings and stratosphere-troposphere coupling to quadrupled CO_2 concentrations in CMIP6 models. *Journal of Geophysical Research: Atmospheres*, **125 (6)**, e2019JD032 345.

Baldwin, M. P., and Coauthors, 2021: Sudden stratospheric warmings. *Reviews of Geophysics*, **59 (1)**, e2020RG000 708.

Bauer, S. E., and Coauthors, 2020: Historical (1850–2014) aerosol evolution and role on climate forcing using the GISS ModelE2. 1 contribution to CMIP6. *Journal of Advances in Modeling Earth Systems*, **12 (8)**, e2019MS001 978.

Bellomo, K., M. Angeloni, S. Corti, and J. von Hardenberg, 2021: Future climate change shaped by inter-model differences in Atlantic meridional overturning circulation response. *Nature Communications*, **12 (1)**, 1–10.

Booth, B. B., N. J. Dunstone, P. R. Halloran, T. Andrews, and N. Bellouin, 2012: Aerosols implicated as a prime driver of twentieth-century North Atlantic climate variability. *Nature*, **484 (7393)**, 228–232.

Butler, A. H., D. W. Thompson, and R. Heikes, 2010: The steady-state atmospheric circulation response to climate change–like thermal forcings in a simple general circulation model. *Journal of Climate*, **23 (13)**, 3474–3496.

Ceppi, P., and D. L. Hartmann, 2015: Connections between clouds, radiation, and midlatitude dynamics: A review. *Current Climate Change Reports*, **1 (2)**, 94–102.

Ceppi, P., G. Zappa, T. G. Shepherd, and J. M. Gregory, 2018: Fast and slow components of the extratropical atmospheric circulation response to CO_2 forcing. *Journal of Climate*, **31 (3)**, 1091–1105.

Chiodo, G., and L. M. Polvani, 2019: The response of the ozone layer to quadrupled CO_2 concentrations: Implications for climate. *Journal of Climate*, **32 (22)**, 7629–7642.

Chiodo, G., L. M. Polvani, D. R. Marsh, A. Stenke, W. Ball, E. Rozanov, S. Muthers, and K. Tsigaridis, 2018: The response of the ozone layer to quadrupled CO_2 concentrations. *Journal of Climate*, **31 (10)**, 3893–3907.

Cowan, T., and W. Cai, 2013: The response of the large-scale ocean circulation to 20^{th} century Asian and non-Asian aerosols. *Geophysical Research Letters*, **40 (11)**, 2761–2767.

DallaSanta, K., C. Orbe, D. Rind, L. Nazarenko, and J. Jonas, 2021a: Dynamical and trace gas responses of the quasi-biennial oscillation to increased CO_2. *Journal of Geophysical Research: Atmospheres*, **126 (6)**, e2020JD034 151.

DallaSanta, K., C. Orbe, D. Rind, L. Nazarenko, and J. Jonas, 2021b: Response of the quasi-biennial oscillation to historical volcanic eruptions. *Geophysical Research Letters*, **48 (20)**, e2021GL095 412.

Delworth, T. L., and K. W. Dixon, 2000: Implications of the recent trend in the Arctic/North Atlantic oscillation for the North Atlantic thermohaline circulation. *Journal of Climate*, **13 (21)**, 3721–3727.

Delworth, T. L., and F. Zeng, 2016: The impact of the North Atlantic oscillation on climate through its influence on the Atlantic meridional overturning circulation. *Journal of Climate*, **29 (3)**, 941–962.

Delworth, T. L., F. Zeng, L. Zhang, R. Zhang, G. A. Vecchi, and X. Yang, 2017: The central role of ocean dynamics in connecting the North Atlantic oscillation to the extratropical component of the Atlantic multidecadal oscillation. *Journal of Climate*, **30 (10)**, 3789–3805.

Eyring, V., S. Bony, G. A. Meehl, C. A. Senior, B. Stevens, R. J. Stouffer, and K. E. Taylor, 2016: Overview of the Coupled Model Intercomparison Project Phase 6 (CMIP6) experimental design and organization. *Geoscientific Model Development*, **9 (5)**, 1937–1958.

Garcia, R. R., and W. J. Randel, 2008: Acceleration of the Brewer–Dobson circulation due to increases in greenhouse gases. *Journal of the Atmospheric Sciences*, **65 (8)**, 2731–2739.

Gervais, M., J. Shaman, and Y. Kushnir, 2019: Impacts of the North Atlantic warming hole in future climate projections: Mean atmospheric circulation and the North Atlantic jet. *Journal of Climate*, **32 (10)**, 2673–2689.

Grise, K. M., and L. M. Polvani, 2014: The response of midlatitude jets to increased CO_2: Distinguishing the roles of sea surface temperature and direct radiative forcing. *Geophysical Research Letters*, **41 (19)**, 6863–6871.

Isaksen, I. S., and Coauthors, 2009: Atmospheric composition change: Climate–chemistry interactions. *Atmospheric Environment*, **43 (33)**, 5138–5192.

Kantha, L. H., and C. A. Clayson, 2000: *Small scale processes in geophysical fluid flows*. Elsevier.

Kelley, M., and Coauthors, 2020: GISS-E2. 1: Configurations and climatology. *Journal of Advances in Modeling Earth Systems*, **12 (8)**, e2019MS002 025.

Khatri, H., R. G. Williams, T. Woollings, and D. M. Smith, 2022: Fast and slow subpolar ocean responses to the North Atlantic oscillation: Thermal and dynamical changes. *Geophysical Research Letters*, **49 (24)**, e2022GL101 480.

Li, F., and P. A. Newman, 2022: Prescribing stratospheric chemistry overestimates southern hemisphere climate change during austral spring in response to quadrupled CO_2. *Climate Dynamics*, 1–18.

Lindzen, R. S., 1987: On the development of the theory of the QBO. *Bulletin of the American Meteorological Society*, 329–337.

Liu, W., A. V. Fedorov, S.-P. Xie, and S. Hu, 2020: Climate impacts of a weakened Atlantic meridional overturning circulation in a warming climate. *Science Advances*, **6 (26)**, eaaz4876.

Ma, L., T. Woollings, R. G. Williams, D. Smith, and N. Dunstone, 2020: How does the winter jet stream affect surface temperature, heat flux, and sea ice in the North Atlantic? *Journal of Climate*, **33 (9)**, 3711–3730.

Marshall, J., H. Johnson, and J. Goodman, 2001: A study of the interaction of the North Atlantic oscillation with ocean circulation. *Journal of Climate*, **14 (7)**, 1399–1421.

McLinden, C., S. Olsen, B. Hannegan, O. Wild, M. Prather, and J. Sundet, 2000: Stratospheric ozone in 3-D models: A simple chemistry and the cross-tropopause flux. *Journal of Geophysical Research: Atmospheres*, **105 (D11)**, 14 653–14 665.

Meinshausen, M., and Coauthors, 2020: The shared socio-economic pathway (SSP) greenhouse gas concentrations and their extensions to 2500. *Geoscientific Model Development*, **13 (8)**, 3571–3605.

Meraner, K., S. Rast, and H. Schmidt, 2020: How useful is a linear ozone parameterization for global climate modeling? *Journal of Advances in Modeling Earth Systems*, **12 (4)**, e2019MS002 003.

Miller, R. L., and Coauthors, 2021: Cmip6 historical simulations (1850–2014) with GISS-E2. 1. *Journal of Advances in Modeling Earth Systems*, **13 (1)**, e2019MS002 034.

Mitevski, I., C. Orbe, R. Chemke, L. Nazarenko, and L. M. Polvani, 2021: Non-monotonic response of the climate system to abrupt CO_2 forcing. *Geophysical Research Letters*, **48 (6)**, e2020GL090 861.

Muthers, S., C. C. Raible, E. Rozanov, and T. F. Stocker, 2016: Response of the AMOC to reduced solar radiation–the modulating role of atmospheric chemistry. *Earth System Dynamics*, **7 (4)**, 877–892.

Nowack, P. J., N. Luke Abraham, A. C. Maycock, P. Braesicke, J. M. Gregory, M. M. Joshi, A. Osprey, and J. A. Pyle, 2015: A large ozone-circulation feedback and its implications for global warming assessments. *Nature Climate Change*, **5 (1)**, 41–45.

O'Callaghan, M. J. D. S., Amee, and D. Mitchell, 2014: The effects of different sudden stratospheric warming types on the ocean. *Geophysical Research Letters*, **41 (21)**, 7739–7745.

Orbe, C., and Coauthors, 2020: GISS Model E2.2: A climate model optimized for the middle atmosphere—2. Validation of large-scale transport and evaluation of climate response. *Journal of Geophysical Research: Atmospheres*, **125 (24)**, e2020JD033 151.

Orbe, C., and Coauthors, 2023: Atmospheric response to a collapse of the North Atlantic circulation under a mid-range future climate scenario: A regime shift in Northern Hemisphere dynamics. *Journal of Climate*.

Reichler, T., J. Kim, E. Manzini, and J. Kröger, 2012: A stratospheric connection to Atlantic climate variability. *Nature Geoscience*, **5 (11)**, 783–787.

Rind, D., J. Jonas, N. Balachandran, G. A. Schmidt, and J. Lean, 2014: The QBO in two GISS global climate models: 1. Generation of the QBO. *Journal of Geophysical Research: Atmospheres*, **119 (14)**, 8798–8824.

Rind, D., G. A. Schmidt, J. Jonas, R. Miller, L. Nazarenko, M. Kelley, and J. Romanski, 2018: Multicentury instability of the Atlantic meridional circulation in rapid warming simulations with GISS ModelE2. *Journal of Geophysical Research: Atmospheres*, **123 (12)**, 6331–6355.

Rind, D., R. Suozzo, N. Balachandran, A. Lacis, and G. Russell, 1988: The GISS global climate-middle atmosphere model. Part I: Model structure and climatology. *Journal of the Atmospheric Sciences*, **45 (3)**, 329–370.

Rind, D., and Coauthors, 2020: GISS Model E2.2: A climate model optimized for the middle atmosphere—model structure, climatology, variability, and climate sensitivity. *Journal of Geophysical Research: Atmospheres*, **125 (10)**, e2019JD032 204.

Roach, L. A., E. Blanchard-Wrigglesworth, S. Ragen, W. Cheng, K. C. Armour, and C. M. Bitz, 2022: The impact of winds on AMOC in a fully-coupled climate model. *Geophysical Research Letters*, e2022GL101203.

Romanou, A., and Coauthors, 2023: Stochastic bifurcation of the North Atlantic circulation under a mid-range future climate scenario with the NASA-GISS ModelE. *Journal of Climate*.

Shaw, T., and Coauthors, 2016: Storm track processes and the opposing influences of climate change. *Nature Geoscience*, **9 (9)**, 656–664.

Shaw, T. A., 2019: Mechanisms of future predicted changes in the zonal mean mid-latitude circulation. *Current Climate Change Reports*, **5 (4)**, 345–357.

Shepherd, T. G., 2014: Atmospheric circulation as a source of uncertainty in climate change projections. *Nature Geoscience*, **7 (10)**, 703–708.

Sigmond, M., and J. F. Scinocca, 2010: The influence of the basic state on the Northern Hemisphere circulation response to climate change. *Journal of Climate*, **23 (6)**, 1434–1446.

Simpson, I. R., T. A. Shaw, and R. Seager, 2014: A diagnosis of the seasonally and longitudinally varying midlatitude circulation response to global warming. *Journal of the Atmospheric Sciences*, **71 (7)**, 2489–2515.

Smith, D. M., and Coauthors, 2019: The polar amplification model intercomparison project (PAMIP) contribution to CMIP6: Investigating the causes and consequences of polar amplification. *Geoscientific Model Development*, **12 (3)**, 1139–1164.

Swingedouw, D., P. Ortega, J. Mignot, E. Guilyardi, V. Masson-Delmotte, P. G. Butler, M. Khodri, and R. Séférian, 2015: Bidecadal North Atlantic ocean circulation variability controlled by timing of volcanic eruptions. *Nature Communications*, **6 (1)**, 1–12.

Vallis, G. K., P. Zurita-Gotor, C. Cairns, and J. Kidston, 2015: Response of the large-scale structure of the atmosphere to global warming. *Quarterly Journal of the Royal Meteorological Society*, **141 (690)**, 1479–1501.

Visbeck, M., H. Cullen, G. Krahmann, and N. Naik, 1998: An ocean model's response to North Atlantic oscillation-like wind forcing. *Geophysical Research Letters*, **25 (24)**, 4521–4524.

Voigt, A., and T. A. Shaw, 2015: Circulation response to warming shaped by radiative changes of clouds and water vapour. *Nature Geoscience*, **8 (2)**, 102–106.

Yuval, J., and Y. Kaspi, 2020: Eddy activity response to global warming–like temperature changes. *Journal of Climate*, **33 (4)**, 1381–1404.

Zhai, H. L. J., Xiaoming, and D. P. Marshall, 2014: A simple model of the response of the Atlantic to the North Atlantic oscillation. *Journal of Climate*, **27 (11)**, 4052–4069.

Zhang, X., D. Waugh, and C. Orbe, 2023: Response of tropospheric transport to abrupt CO_2 increase: Dependence on the Atlantic Meridional Overturning Circulation. *Journal of Geophysical Research: Atmospheres*.